Published in final edited form as:
J Phys Chem C Nanomater Interfaces. 2009 ; 113(7): 2676–2684. doi:10.1021/jp8076672.

Metallic Nanostructures as Localized Plasmon Resonance Enhanced Scattering Probes for Multiplex Dark Field Targeted Imaging of Cancer Cells

Rui Hu, **Ken-Tye Yong**, **Indrajit Roy**, **Hong Ding**, **Sailing He**, and **Paras N. Prasad**
Institute for Lasers, Photonics and Biophotonics, University at Buffalo, The State University of New York, Buffalo, New York 14260-4200, and Centre for Optical and Electromagnetic Research, Zhejiang University, Hangzhou 310058, China

Abstract

In this paper, we report the use of bioconjugated gold nanorods and silver nanoparticles as targeted localized surface plasmon resonance enhanced scattering probes for dark field multiplex and transmission electron microscopy (TEM) imaging of pancreatic cancer cells. We take advantage of the spectrally widely separated localized plasmon resonance of the gold nanorods and silver nanoparticles which produce wavelength selective plasmon resonance scattering to allow multiplex imaging with high contrast. By functionalizing the surfaces, aqueous dispersions of bioconjugated gold nanorods and silver nanoparticles are prepared. We demonstrate receptor-mediated delivery of bioconjugated gold nanorods and silver nanoparticles simultaneously into pancreatic cancer cells, using multiplexed dark field microscopy technique. We also show that the bioconjugated metallic nanostructures can be used for high contrast TEM imaging as well.

Introduction

Nanometer-sized metallic particles have emerged as a new class of materials for applications ranging from physics to biology.[1-13] Metal colloids are well-known for their localized surface plasmon resonance (LSPR) properties, which originate from collective oscillation of their electrons in response to optical excitation.[14] The LSPR frequency of a particular metal colloid has been shown to depend on particle shape, composition and refractive index of the surrounding medium, among many other factors.[15-21] Metallic nanoparticles can be functionalized with biomolecules (e.g. small-molecule drugs, aptamers, peptides, and antibodies) for specific targeting of tumor cells and early detection of cancer.[22-29] Recently, quantum dots have extensively been used for targeting tumor cells and whole animal imaging due to their unique size-dependent luminescent properties.[30,31] However, potential in vivo toxicity of the quantum dots is a major hurdle towards their widespread biological applications, particularly in the clinic.[32-34] On the other hand, metallic nanoparticles are much better suited candidates for biomedical applications due to their ease of synthesis, commercial availability in various size ranges, ready bioconjugation, and most importantly absence of biotoxicity.[35-37]

A considerable effort has been focused on nanoparticles of colloidal gold and silver, for which a broad range of synthetic procedures were reported in terms of tunability of their size, shape, and composition.[38-44] For example, a seed-mediated growth method was most commonly used for fabricating gold nanorods (Au NRs). In this approach, pioneered by Murphy's group, gold nanoparticles were employed to seed the growth of NRs.[45-50] This synthetic route yields colloidally stable and easily functionalizable nanoparticles of high monodispersity and is now commonly used for sensor applications. Typically, Au NRs have two distinct plasmon

resonance absorption bands, a longitudinal band corresponding to electron motion along the long axis of the particle, and the transverse band corresponding to motion along the short axis of the particle.[18,19] The absorption maximum for the longitudinal band shifts to longer wavelengths with the increasing aspect ratio (length/diameter). To date, it has been shown that the longitudinal band can be systematically tuned from ~600 to ~1200 nm.[41,42] Silver nanoparticles (Ag NPs) are another important class of nanomaterials that have been used in catalysis, surface enhanced Raman scattering (SERS), and electronics.[51-53] The synthesis and characterization of Ag NPs have thus attracted considerable attention from both fundamental and practical points of view for the past decade.[16] In general, spherical silver nanoparticles with ~10 nm size have a LSPR peak around 400 nm. Recent studies have demonstrated the use of these metallic nanoparticles (e.g. gold and silver) as contrast agents for biomedical imaging using dark field microscopy, multiphoton plasmon resonance microscopy, optical coherence microscopy, Hyper-Rayleigh scattering spectroscopy, and Raman spectroscopy.[22, 23,25,26,54-58]

Though nanoparticles of several metals have been produced for biological studies, there have been very few reports of using combination of high-quality Au NRs and Ag NPs of controlled size for targeted bioimaging. Recently, El-Sayed's group has showed the use of Au NPs and NRs as novel contrast agents for both in vitro molecular imaging and photothermal cancer therapy.[23] Kotov's group has shown the development of Au NRs as contrast agent for a laser optoacoustic imaging system, which can significantly widen preclinical and clinical applications by using this imaging modality for early detection of cancerous tissues.[59] Xu's group has demonstrated the use of Ag NPs as nanometer size index probes for measurement of real-time changes of membrane permeability and pore size of *P. aeruginosa*.[60] Lakowicz's group has demonstrated fluorescence imaging of cells using silver particle-based plasmon-coupled probes (PCPs) at a single cell resolution.[61-63] These encouraging results on metallic nanoparticles as biological markers or probes and sensors provide a nanoimaging platform for further exploration of ultrasensitive imaging and detection strategies.

Metallic nanoparticles have several advantages for bioimaging when compared to other nanoparticles (e.g. semiconductor and magnetic).[4] Metallic nanoparticles scatter light intensely and they are much brighter than chemical fluorophores. They do not photobleach and they can be easily detected at the single-particle limit. Metallic nanoparticles exhibit enhanced scattering at wavelengths of their localized plasmon resonance. To our knowledge, no literature has reported using combination of Au NRs and Ag NPs for multiplex imaging.[64,65] Thus wavelength selective scattering from metallic nanoparticles offers potential for multiplexed bioimaging studies using a single white light source.[43]

We demonstrate here LSPR enhanced wavelength selective scattering from Au NRs and Ag NPs for targeted high contrast multiplex imaging of human pancreatic cancer cells. Antibodies such as anti-claudin 4 (aC4) and anti-mesothelin (aMe), whose corresponding antigen receptors (claudin 4 and mesothelin) are known to be overexpressed in both primary and metastatic pancreatic cancer, were utilized for the synthesis of bioconjugates of Au NRs and Ag NPs. The biocompatible polyelectrolyte coated Au NRs and Ag NPs were conjugated with antibodies by electrostatic interaction. According to our knowledge, no study has been reported on the use of combination of Au NR and Ag NP bioconjugates as targeted plasmon enhanced scattering probes for multiplex dark field imaging of live cancer cells. With dark field microscopy, we show receptor-mediated uptake of Au NR and Ag NP bioconjugates into pancreatic cancer cells in vitro. More importantly, we have found that the polymer coated Au NRs and Ag NPs have very low cytotoxic effect, thereby justifying our future strategy of using them for targeted in vivo bioimaging.

Experimental Methods

Materials

Cetyltrimethylammonium bromide (CTAB, H-5882), L-ascorbic acid (AA), silver nitrate (AgNO3), nitric acid (HNO3), sodium chloride (NaCl), hydrogen tetrachloroaurate(III) trihydrate ($HAuCl4{\cdot}3H_2O$) and sodium borohydride ($NaBH_4$) were purchased from Aldrich. All chemicals were used as received without any purification. HPLC-grade water was used in all the experiments. Poly(3,4-ethylenedioxythiophene)-poly(styrenesulfonate) (PEDT/PSS, molecular weight = 240,000), and Poly(diallyldimethylammonium chloride) (PDDAC, 20%) were purchased from Polysciences, Inc. Anti-claudin-4 and anti-mesothelin were purchased from Invitrogen.

Synthesis of gold nanorods with different aspect ratios

The gold seeds were synthesized by the method described by Nikoobakht et al. Briefly, 5 ml of 0.2 M CTAB solution was mixed with 5 ml of 0.96 mM $HAuCl_4$. 0.80 ml of ice-cold 0.01 M $NaBH_4$ was quickly added, with stirring, resulting in the formation of a light-brown solution. The seed solution was vigorously stirred for 2 min and then kept at 33°C for 30 minutes before use. This seed solution was used for the synthesis of gold NRs after 30 minutes. The average size of these gold seeds was ~ 4 nm. In a separate vial, 5.0 mL of 0.96 mM $HAuCl_4$ and 100 μL of 0.1 M ascorbic acid were added to 5.0 mL of 0.2 M CTAB solution at room temperature. Suitable additive (e.g. silver nitrate, sodium chloride, and nitric acid) was then individually added to this solution to tailor the aspect ratio of the rod particles and it was gently mixed for 15 to 30 seconds. We refer to this mixture as the growth solution. The growth solution was then placed in a water bath at 33°C. Next, 12 μL of the seed solution was added to the growth solution. The resulting mixture was left undisturbed and aged for ~5 hours in the water bath. Au NRs were concentrated and separated from the excess surfactant solution by centrifugation.

Synthesize of silver nanoparticles

Silver nanoparticles were prepared by directly reducing AgNO3 with $NaBH_4$ in the presence of sodium citrate. Briefly, 1.0 mL of freshly prepared ice-cold $NaBH_4$ solution was added into a mixture of silver nitrate (0.5 mM) and sodium citrate (2 mM) solution under vigorous stirring. After 30 minutes of stirring, the Ag NPs were separated and purified by centrifugation.

Fabrication of biocompatible polymer coated gold nanorods and silver nanoparticles

The assynthesized Au NRs were capped with a bilayer of CTAB, which is positively charged. These NRs were centrifuged at 7000 rpm to remove excess CTAB. Then, the positively charged surface of NRs was changed to a negatively charged one by coating the NRs with PEDT/PSS polyelectrolyte solution. After one hour of treatment, the extra PEDT/PSS was separated by centrifugation. Following that, using the same approach, the negative charged surface of NRs were re-converted to positive charge by further coating with a layer of PDDAC polyelectrolyte. As for Ag NPs, the as-fabricated Ag NP surface was covered with a layer of citrate molecules, which is negatively charged. Then, the negatively charged surface of NPs was changed to a positively charged one by using the same approach mentioned above. These polyelectrolyte coated nanoparticles were found to be highly non-toxic and were colloidally stable in aqueous phase for months. For simplicity, we refer to Au NRs or Ag NPs coated with positive (PDDAC) or negative (PEDT/PSS) charged polyelectrolyte as (+)pdNRs, (-)peNRs, (+)pdNPs, and (-)peNPs, respectively.

Conjugating targeting molecules to gold nanorods and silver nanoparticles

For conjugating transferrin to the particles, the cationic PDDAC-capped Au NRs or Ag NPs solution (~50 μg/ml) were mixed with Tf solution (40 mg/ml) at a volume ratio of 10:1, and

was allowed to react for 30 to 60 min. The Tf probably linked to the PDDAC-coated NRs or NPs by electrostatic interaction. In the case of conjugating antibodies, negatively charged particles were used. Basically, the anionic PEDT/PSS-capped Au NRs or Ag NPs solution (~50 μg/ml) were mixed with antibody solution (0.5 mg/ml) at a volume ratio of 100:1 and was allowed to react for an hour.

Cell labeling studies

The cells were obtained as described previously and maintained in DMEM medium with 10% fetal bovine serum (FBS) and appropriate antibiotic. The day prior to treatment, cells were seeded on a square glass cover slip in 35 mm cell culture dishes at 40~50% confluence. Cells were treated with Tf- or antibody-conjugated nanorods or nanoparticles at a final concentration of 2~3 μg/ml on the day of treatment. The samples were incubated for 14 to 16 hrs before imaging.

UV-Visible absorbance

The absorption spectra were collected using an Agilent 8453 UV-Visible spectrophotometer over the range from 300 to 1100 nm. The samples were measured against water as reference. All samples were loaded into a quartz cell for measurements.

Transmission electron microscopy (TEM)

Transmission Electron Microscopy (TEM) images were obtained using a JEOL model JEM-100CX microscope with an acceleration voltage of 100 kV. The specimens were prepared by drop-coating the sample dispersion onto a carbon coated 300 mesh copper grid, which was placed on filter paper to absorb excess solvent.

Dark field Microscopy

The dark field images were recorded using an upright Nikon Eclipse 800 microscope with a high numerical dark field condenser (N.A. 1.20-1.43, oil immersion) and a 100X/ 1.4 NA oil Iris objective (Cfi Plan Fluor). In the dark field configuration, the condenser delivers a narrow beam of white light from a tungsten lamp and the high NA oil immersion objective collects only the scattered light from the samples. The iris of the objective can be adjusted to optimize the collection and to reduce the leakage of transmitted light. The dark field imaging was captured using a QImaging Micropublisher 3.3 RTV color camera. A 0.5x lens was placed in front of the camera to provide a larger view of the field. The Qcapture software from the camera manufacturer was used for image acquisition and has a feature for adjusting the white color balance for accurately capturing the color differences in samples.

Cell viability study

For each MTS (3-(4,5-dimethylthiazol-2-yl)-5-(3-carboxymethoxyphenyl)-2-(4-sulfophenyl)-2H-tetrazolium, inner salt) assay,[66] 96 culture wells of Panc-1 cells were prepared (5000 cells in each of 96 wells). Four sets were treated with different concentration of functionalized Au NRs (or Ag NPs) and one set served as the non-treated control. The complete assay was performed thrice, and results were averaged. Various concentrations of Au NRs (or Ag NPs) ranging from 600 to 9600 μg/mL, were added to each well and subsequently incubated with the cells for 48 h at 37 °C under 5% CO_2. As described in the literature, the absorbance of formazan (produced by the cleavage of MTS by dehydrogenases in living cells) is directly proportional to the number of live cells. After the incubation, 10 μL of MTS reagent was then added to each well and thoroughly mixed. One hour later, the absorbance of the mixtures at 490 nm was measured using a multiwell plate reader. The cell viability was calculated as the ratio of the absorbance of the sample well to that of the control well and expressed as a percentage viability, assigning the viability of non-treated cells as 100%. For statistical

analysis, comparison between two groups was analyzed by the two-tailed Student's t-test statistical software (SPSS). Values are presented as mean ± SD (n=4). A difference of $P<0.05$ was considered statistically significant.

Results and Discussion

Scheme 1 illustrates the surface functionalization and conjugation of Au NRs and Ag NPs for cellular targeting and imaging. In this case we have employed polyelectrolytes, which have been extensively used for the colloidal stabilization and surface functionalization of NPs. It was shown that the polyelectrolyte coating of carboxylic acid-derivatized Au NPs has been achieved by electrostatic self-assembly of oppositely charged polyelectrolytes.[23] More importantly, they have been found to be biocompatible and possess low toxicity.[25,67] The first step involves a surface coating process of charged nanoparticles with polyelectrolyte. Since the as-prepared Au NRs were coated by a positively charged CTAB bilayer, which is known for its cytotoxicity, they were coated first by a negatively charged polyelectrolyte PEDT/PSS. In order to convert the resulting anionic Au NRs to cationic Au NRs, a positively charged polyelectrolyte PDDAC was used as the next coating material (Scheme 1a). A similar strategy was applied to Ag NPs, the only difference being that the as-prepared Ag NPs were stabilized by negatively charged sodium citrate. After coating, the polyelectrolyte-coated NRs or NPs are water-dispersible and non-toxic. Next, the polyelectrolyte-coated particles were conjugated with a monoclonal antibody (negatively charged particles were used here) or transferrin (positively charged particles were used here) by using simple electrostatic interaction. The prepared bioconjugates were then used for targeted labeling of pancreatic cancer cells. It is worth noting that for small particles, such as Ag NPs with a diameter around 10nm, several particles may be capped together by the polyelectrolyte to form a single large particle, as demonstrated in scheme 1b.

The functionalized Au NRs and Ag NPs were systematically characterized by UV-Visible spectroscopy, transmission electron microscopy (TEM), and dark field microscopy. We prepared Au NRs by a one-step seed-mediated growth method that uses suitable additives (e.g. $AgNO_3$, NaCl, KCl or HNO_3) to fine-tune the NR's aspect ratio, shape, and structure, and thereby the optical properties.[45,50] Figure 1 shows the effect of introducing different additives into identical growth solutions on the absorption spectra of the resulting Au NRs. With systematically tuning the additive concentration, the longitudinal plasmon band red-shifts from ~620 to ~900 nm (Figure 1). We have observed that the aspect ratio of the NRs increases as the longitudinal surface plasmon peak position increases, which is consistent with previous references. Figure 2 shows the TEM images of several different nanoparticulate specimens. Figure 3 shows the absorption spectra of the functionalized Ag NPs, Au NPs and Au NRs and their corresponding light scattering images. The light scattering images of Ag NPs, Au NPs and Au NRs in the bottom right were taken from a dark field optical microscope. The orange/red scattering associated with the Au NRs, as seen in Figure 3, originates from their strong longitudinal surface plasmon oscillation which has a resonant frequency within the red region of the optical spectrum. This plasmon-enhanced scattering from Au NRs is much brighter than the fluorescence from most fluorophores. On the other hand, Ag (Au) NPs have a blue (green) scattering feature that has a resonance frequency within the blue (green) region. Figure 4 shows the change in the ζ-potential of the Au NRs before and after functionalizing. From Figure 4, charge reversal could be easily observed upon coating with each of the anionic and cationic polyelectrolytes. A small change in the ζ-potential value after antibody conjugation is probably due to the almost neutral property of the antibody. On the other hand, since transferrin (Tf) has an excess of carboxyl groups, a greater change in the ζ-potential value was observed after Tf-conjugation.

In this study, dynamic light scattering (DLS) was used to determine the colloidal stability of the CTAB capped Au NRs (Au (+)ctNRs), Au (-)peNRs and Au (+)pdNRs, dispersed in glucose solution (5%). The time-dependent profile of the effective diameter of the Au (+)ctNRs, Au (-)peNRs and Au (+)pdNRs is shown in Figure 5. Over the time range from 0 to 800 minutes, the effective diameter varies by less than 10%, suggesting that their colloidal stability is not affected by the glucose solution. In addition, an increase in the diameters of these Au NRs after being coated with polyelectrolyte is observed which indicates successful polyelectrolyte coatings after each step. It is worth mentioning that the size of the Au (+)ctNRs is ~40nm in length and ~15nm in width, and the light scattering data shows a total hydrodynamic diameter of ~19nm. However, the light-scattering analysis only provides an average spherical diameter. Thus, the actual sizes determined by light scattering in our case cannot be taken literally. Therefore, we want to emphasize that the light-scattering technique used here is only to demonstrate non-aggregation of the NRs under different physiological conditions.

The Tf-conjugated Au (+)pdNRs and Ag (+)pdNPs were then used for in vitro imaging using dark field microscopy. Human pancreatic cancer cells (e.g. Panc-1 and MiaPaCa) are chosen as the target cell lines, which are known to overexpress transferrin receptors (TfRs), as well as claudin-4 and mesothelin antigen receptors. Figure 6 shows MiaPaCa cells stained with Tf-conjugated Au (+)pdNRs or Ag (+)pdNPs bioconjugates. Robust receptor-mediated cellular uptake is demonstrated from the dark field images of MiaPaCa cells treated with the Tf-Au (+)pdNRs (the orange/red scattering color) and Tf-Ag (+)pdNPs (the blue/green scattering color). The Tf-Au (+)pdNRs and the Tf-Ag (+)pdNPs bioconjugates appear to accumulate in vesicles within the cells, suggesting an endocytotic uptake. Control experiments were performed to verify that bioconjugates are specifically taken up through the Tf-TfR interaction. In the control experiment, the cells were incubated with non-bioconjugated Au (+)pdNRs and Ag (+)pdNPs. In this case, a minimal uptake of particles was observed, confirming the specific receptor-mediated nature of the uptake of the bioconjugated nanoparticles/rods.

Figure 7 illustrates labeling two different pancreatic cancer cell types (Panc-1 and MiaPaCa) with the four types of bioconjugates, anti-claudin 4 conjugated Au NRs (aC4-Au NRs), anti-mesothelin conjugated Au NRs (aMe-Au NRs), anti-claudin 4 conjugated Ag NPs (aC4-Ag NPs), and anti-mesothelin conjugated Ag NPs (aMe-Ag NPs). Cellular uptake of the bioconjugates can be clearly observed from the robust optical signals of the Panc-1 and MiaPaCa cells, while a much lower signal is observed in the case of cells treated with non-bioconjugated particles (data not shown), which demonstrates the specific nature of antibody-mediated targeting on the pancreatic cancer cells. This is a promising demonstration of receptor-mediated targeting of functionalized NRs and NPs to pancreatic cancer cells, which is an improvement over previous attempts for targeted plasmonic scattering imaging using bioconjugated gold nanoparticles, where no preferential cellular uptake over non-targeted gold nanoparticles was reported. [25]

Based on the successful imaging result with Panc-1 and MiaPaCa cells, we further proved that functionalized Au (-)peNRs and Ag (-)peNPs with different LSPR wavelengths can be used as an effective optical indicator to identify a specific type of cancer cell, using conjugated biomolecules targeting the overexpressed receptors present on the cell type. Our method of identifying specific pancreatic cancer cells is straightforward. In this experiment, both Au (-)peNRs and Ag (-)peNPs were conjugated with anti-mesothelin for specific targeting of human pancreatic cancer cells (Panc-1). Here, cellular labeling with the Au NR and Ag NP bioconjugates are expected to dominate over that of their non-bioconjugated counterparts, owing to the affinity of anti-mesothelin for these cells. Indeed, Figure 8 shows a dark field image of Panc-1 cells that are stained with both the Au NRs and Ag NPs bioconjugates. Light scattering colors (Figure 8, Insets) from the overall staining of bioconjugates on the cells indicates that the scattering signal indeed originated both from the Au NRs and Ag NPs.

Another advantage of using metallic nanostructures is that owing to their high electron density, they can also serve as excellent contrast agents for transmission electron microscopic (TEM) imaging. Intracellular uptake of antibody conjugated Au NRs and Ag NPs was further confirmed by using TEM. Figure 9 recorded the electron microscopy images of Panc-1 cells after 16 hours of treatment with aMe-Au NRs and aMe-Ag NPs. The Au NRs and Ag NPs located within several intracellular vesicles evidently show that the antibody conjugated Au NRs and Ag NPs were avidly uptaken by Panc-1 cells. Thus Figure 9 demonstrates that metallic nanostructures can also be used as nonoptical contrast agents for TEM.

Besides using the functionalized metallic particles as biomarkers, we have also systematically investigated their possible cytotoxic effects on the Panc-1 cell line. Figure 10 shows the results of a cell viability assay following treatment of Panc-1 cells with Au (-)peNRs, Au (+)pdNRs, Ag (-)peNPs and Ag (+)pdNPs in vitro. It is seen that all the bioconjugates maintained greater than 80% cell viability even for particle concentration as high as ~1000μg/ml for both Au (+) pdNRs and Au (-)peNRs and ~500μg/ml for both Ag (+)pdNPs and Ag (-)peNPs, respectively. As shown in Figure 10, the 50% cell viabilities (IC50's) are 720μg/ml, 1800μg/ml, 9600μg/ml and 9600μg/ml for Ag (+)pdNPs, Ag (-)peNPs, Au (+)pdNRs and Au (-)peNRs, respectively. This indicates that such bioconjugates have negligible in vitro toxicity and can be used as efficient targeted contrast agents for molecular whole body imaging.

The distinct absorption spectra between Au NRs and Ag NPs in the visible and the near-IR regions of the electromagnetic spectrum provide many excellent opportunities for detection and therapy of human cancer. For example, it is known that pancreatic tumor overexpresses EGFR receptors on the cell membrane. Targeting anti-EGFR conjugated Au NRs on the cell surface allows for selective photothermal therapy with a near-infrared laser. The strong scattering of gold and silver nanoparticles enables them to be efficient image contrast agents. Thus, metallic nanoparticles offer a combination of diagnostic and therapeutic modalities in biomedical imaging and cancer therapy.

Conclusions

In conclusion, we have engineered biocompatible functionalized Au NRs and Ag NPs for targeted labeling of pancreatic cancer cells in vitro by a facile method. These polyelectrolye-coated Au NRs and Ag NPs can be conjugated with monoclonal antibodies and proteins by simple electrostatic interaction. We have used the spectrally well separated LSPR features of Au NRs and Ag NPs to demonstrate high contrast multiplex imaging using dark field microscope. We have shown the robust labeling of Au NR and Ag NP bioconjugates in pancreatic cancer cells such as Panc-1 and MiaPaCa. These findings not only offer insights into the receptor-mediated delivery mechanism using multiplexed imaging, but also help the design and development of future nanoprobes for in vivo imaging and therapeutic applications. By combining the scattering brightness and biocompatibility of metallic nanoparticles, we believe that these nanoparticles will serve as a new generation of contrast agents for early diagnosis of human cancer.

Acknowledgment

This study was supported by grants from NCI CA119397, NY Center of Excellence, U. S. Air Force of Scientific Research, and the John R. Oishei Foundation. K. T. Y. is supported by the AACR-Pancreatic Cancer Action Network Fellowship for Pancreatic Cancer Research.

References and Notes

(1). Prasad, PN. Nanophotonics. Wiley-Interscience; New York: 2004.

(2). Prasad, PN. Introduction to Biophotonics. Wiley-Interscience; New York: 2004.

(3). Ahmadi TS, Wang ZL, Green TC, Henglein A, El-Sayed MA. Science 1996;272:1924. [PubMed: 8662492]
(4). Jain PK, Huang X, El-Sayed IH, El-Sayed MA. Acc. Chem. Res. 2008
(5). Elghanian R, Storhoff JJ, Mucic RC, Letsinger RL, Mirkin CA. Science 1997;277:1078. [PubMed: 9262471]
(6). Nie S, Emory SR. Science 1997;275:1102. [PubMed: 9027306]
(7). Cao YC, Jin R, Mirkin CA. Science 2002;297:1536. [PubMed: 12202825]
(8). Sonnichsen C, Reinhard BM, Liphardt J, Alivisatos AP. Nat Biotech 2005;23:741.
(9). Jain PK, El-Sayed IH, El-Sayed MA. Nano Today 2007;2:18.
(10). Qian X, Peng X-H, Ansari DO, Yin-Goen Q, Chen GZ, Shin DM, Yang L, Young AN, Wang MD, Nie S. Nat Biotech 2008;26:83.
(11). Biesso A, Qian W, El-Sayed MA. J. Am. Chem. Soc 2008;130:3258. [PubMed: 18290646]
(12). Oyelere AK, Chen PC, Huang X, El-Sayed IH, El-Sayed MA. Bioconjugate Chem 2007;18:1490.
(13). Rosi NL, Giljohann DA, Thaxton CS, Lytton-Jean AKR, Han MS, Mirkin CA. Science 2006;312:1027. [PubMed: 16709779]
(14). Mulvaney P. Langmuir 1996;12:788.
(15). El-Sayed MA. Acc. Chem. Res 2001;34:257. [PubMed: 11308299]
(16). Burda C, Chen X, Narayanan R, El-Sayed MA. Chem. Rev 2005;105:1025. [PubMed: 15826010]
(17). Yu YY, Chang SS, Lee CL, Wang CRC. J. Phys. Chem. B 1997;101:6661.
(18). Link S, El-Sayed MA. International Reviews in Physical Chemistry 2000;19:409.
(19). Link S, Mohamed MB, El-Sayed MA. J. Phys. Chem. B 1999;103:3073.
(20). Link S, El-Sayed MA. J. Phys. Chem. B 1999;103:8410.
(21). Jain PK, Lee KS, El-Sayed IH, El-Sayed MA. J. Phys. Chem. B 2006;110:7238. [PubMed: 16599493]
(22). El-Sayed IH, Huang X, El-Sayed MA. Nano Lett 2005;5:829. [PubMed: 15884879]
(23). Huang X, El-Sayed IH, Qian W, El-Sayed MA. J. Am. Chem. Soc 2006;128:2115. [PubMed: 16464114]
(24). Agarwal A, Huang SW, Donnell MO, Day KC, Day M, Kotov N, Ashkenazi S. Journal of Applied Physics 2007;102:064701.
(25). Ding H, Yong KT, Roy I, Pudavar HE, Law WC, Bergey EJ, Prasad PN. J. Phys. Chem. C 2007;111:12552.
(26). Durr NJ, Larson T, Smith DK, Korgel BA, Sokolov K, Ben-Yakar A. Nano Lett 2007;7:941. [PubMed: 17335272]
(27). Huang X, El-Sayed IH, Qian W, El-Sayed MA. Nano Lett 2007;7:1591. [PubMed: 17474783]
(28). Huang X, Qian W, El-Sayed IH, El-Sayed MA. Lasers in Surgery and Medicine 2007;39:747. [PubMed: 17960762]
(29). Tong L, Zhao Y, Huff TB, Hansen MN, Wei A, Cheng J-X. Advanced Materials 2007;19:3136. [PubMed: 19020672]
(30). Klostranec JM, Chan WCW. Advanced Materials 2006;18:1953.
(31). Alivisatos P. Nat Biotech 2004;22:47.
(32). Gao X, Yang L, Petros JA, Marshall FF, Simons JW, Nie S. Current Opinion in Biotechnology 2005;16:63. [PubMed: 15722017]
(33). Derfus AM, Chan WCW, Bhatia SN. Nano Lett 2004;4:11.
(34). Michalet X, Pinaud FF, Bentolila LA, Tsay JM, Doose S, Li JJ, Sundaresan G, Wu AM, Gambhir SS, Weiss S. Science 2005;307:538. [PubMed: 15681376]
(35). Lee KS, El-Sayed MA. J. Phys. Chem. B 2006;110:19220. [PubMed: 17004772]
(36). Connor EE, Mwamuka J, Gole A, Murphy CJ, Wyatt MD. Small 2005;1:325. [PubMed: 17193451]
(37). Hauck TS, Ghazani AA, Chan WCW. Small 2008;4:153. [PubMed: 18081130]
(38). Jana NR, Gearheart L, Murphy CJ. Chemical Communications 2001:617.
(39). Kim F, Song JH, Yang P. J. Am. Chem. Soc 2002;124:14316. [PubMed: 12452700]
(40). Sun Y, Xia Y. Science 2002;298:2176. [PubMed: 12481134]

(41). Sau TK, Murphy CJ. J. Am. Chem. Soc 2004;126:8648. [PubMed: 15250706]
(42). Pérez-Juste J, Pastoriza-Santos I, Liz-Marzána LM, Mulvaney P. Coordination Chemistry Reviews 2005;249:1870.
(43). Orendorff CJ, Sau TK, Murphy CJ. Small 2006;2:636. [PubMed: 17193100]
(44). Link S, Burda C, Nikoobakht B, El-Sayed MA. J. Phys. Chem. B 2000;104:6152.
(45). Busbee BD, Obare SO, Murphy CJ. Advanced Materials 2003;15:414.
(46). Pérez-Juste J, Liz-Marzán LM, Carnie S, Chan DYC, Mulvaney P. Advanced Functional Materials 2004;14:571.
(47). Sau TK, Murphy CJ. Langmuir 2004;20:6414. [PubMed: 15248731]
(48). Gou L, Murphy CJ. Chem. Mater 2005;17:3668.
(49). Smith DK, Korgel BA. Langmuir 2008;24:644. [PubMed: 18184021]
(50). Yong K-T, Sahoo Y, Swihart MT, Schneeberger PM, Prasad PN. Topics in Catalysis 2008;47:49.
(51). Murphy CJ, Gole AM, Hunyadi SE, Stone JW, Sisco PN, Alkilany A, Kinard BE, Hankins P. Chemical Communications 2008:544. [PubMed: 18209787]
(52). Kneipp K, Kneipp H, Itzkan I, Dasari RR, Feld MS. Chem. Rev 1999;99:2957. [PubMed: 11749507]
(53). Haes AJ, Van Duyne RP. J. Am. Chem. Soc 2002;124:10596. [PubMed: 12197762]
(54). Troutman TS, Barton JK, Romanowski M. Opt. Lett 2007;32:1438. [PubMed: 17546147]
(55). Wang H, Huff TB, Zweifel DA, He W, Low PS, Wei A, Cheng J-X. Proceedings of the National Academy of Sciences 2005;102:15752.
(56). Cang H, Sun T, Li Z-Y, Chen J, Wiley BJ, Xia Y, Li X. Opt. Lett 2005;30:3048. [PubMed: 16315717]
(57). Darbha GK, Rai US, Singh AK, Ray PC. Chemistry - A European Journal 2008;14:3896.
(58). Jana NR, Pal T. Advanced Materials 2007;19:1761.
(59). Eghtedari M, Oraevsky A, Copland JA, Kotov NA, Conjusteau A, Motamedi M. Nano Lett 2007;7:1914. [PubMed: 17570730]
(60). Xu XHN, Brownlow WJ, Kyriacou SV, Wan Q, Viola JJ. Biochemistry 2004;43:10400. [PubMed: 15301539]
(61). Zhang J, Fu Y, Chowdhury MH, Lakowicz JR. Nano Lett 2007;7:2101. [PubMed: 17580926]
(62). Zhang J, Fu Y, Lakowicz JR. Bioconjugate Chem 2007;18:800.
(63). Zhang J, Fu Y, Liang D, Nowaczyk K, Zhao RY, Lakowicz JR. Nano Lett 2008;8:1179. [PubMed: 18341300]
(64). Yu C, Irudayaraj J. Analytical Chemistry 2007;79:572. [PubMed: 17222022]
(65). Yu C, Nakshatri H, Irudayaraj J. Nano Letters 2007;7:2300. [PubMed: 17602538]
(66). Cory AH, O. T, Barltrop JA, Cory JG. Cancer Communications 1991;3:207. [PubMed: 1867954]
(67). Gole A, Murphy CJ. Chem. Mater 2005;17:1325.

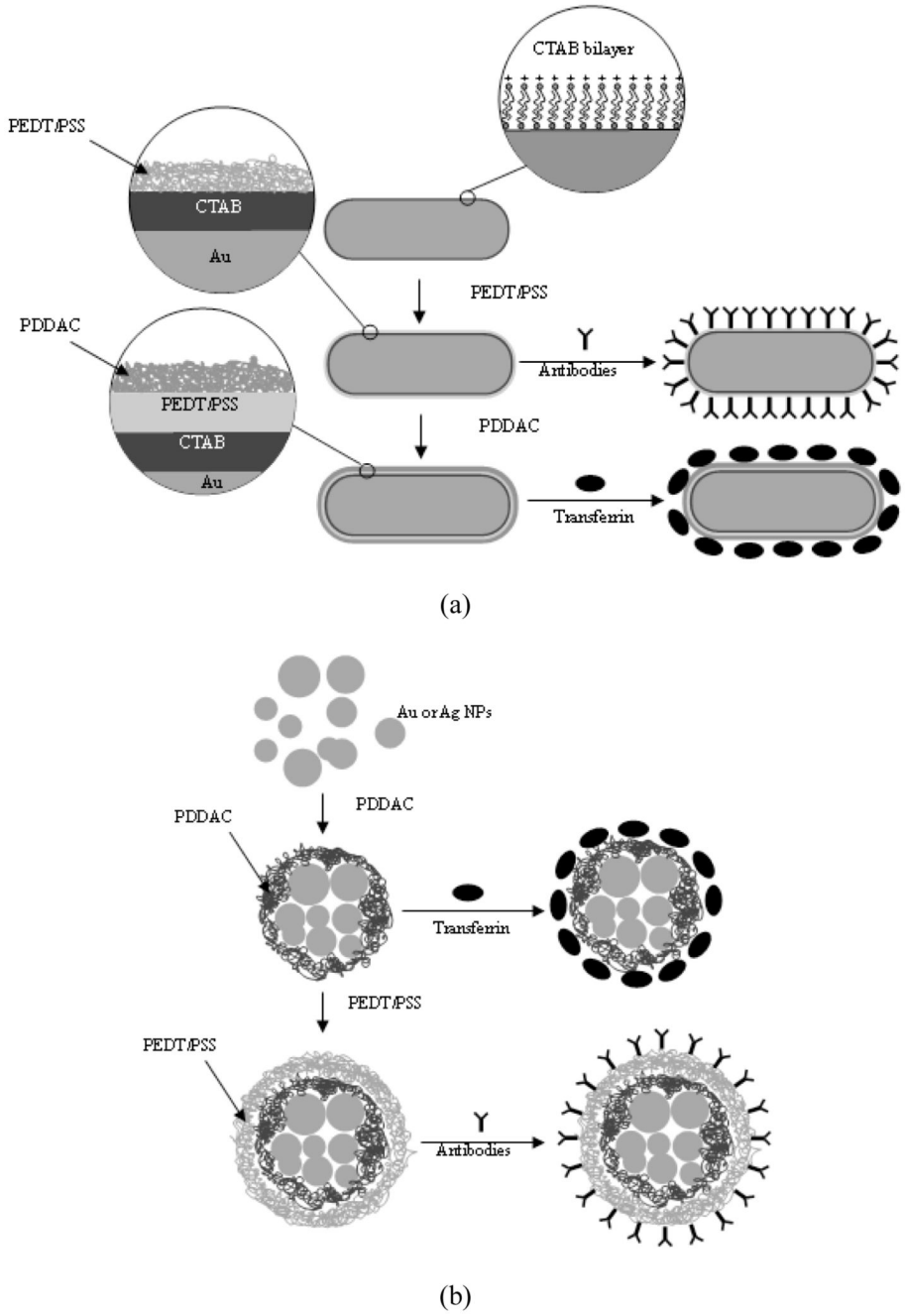

Scheme 1.
Surface functionalization and conjugation of Au NRs (a) and Ag or Au NPs (b).

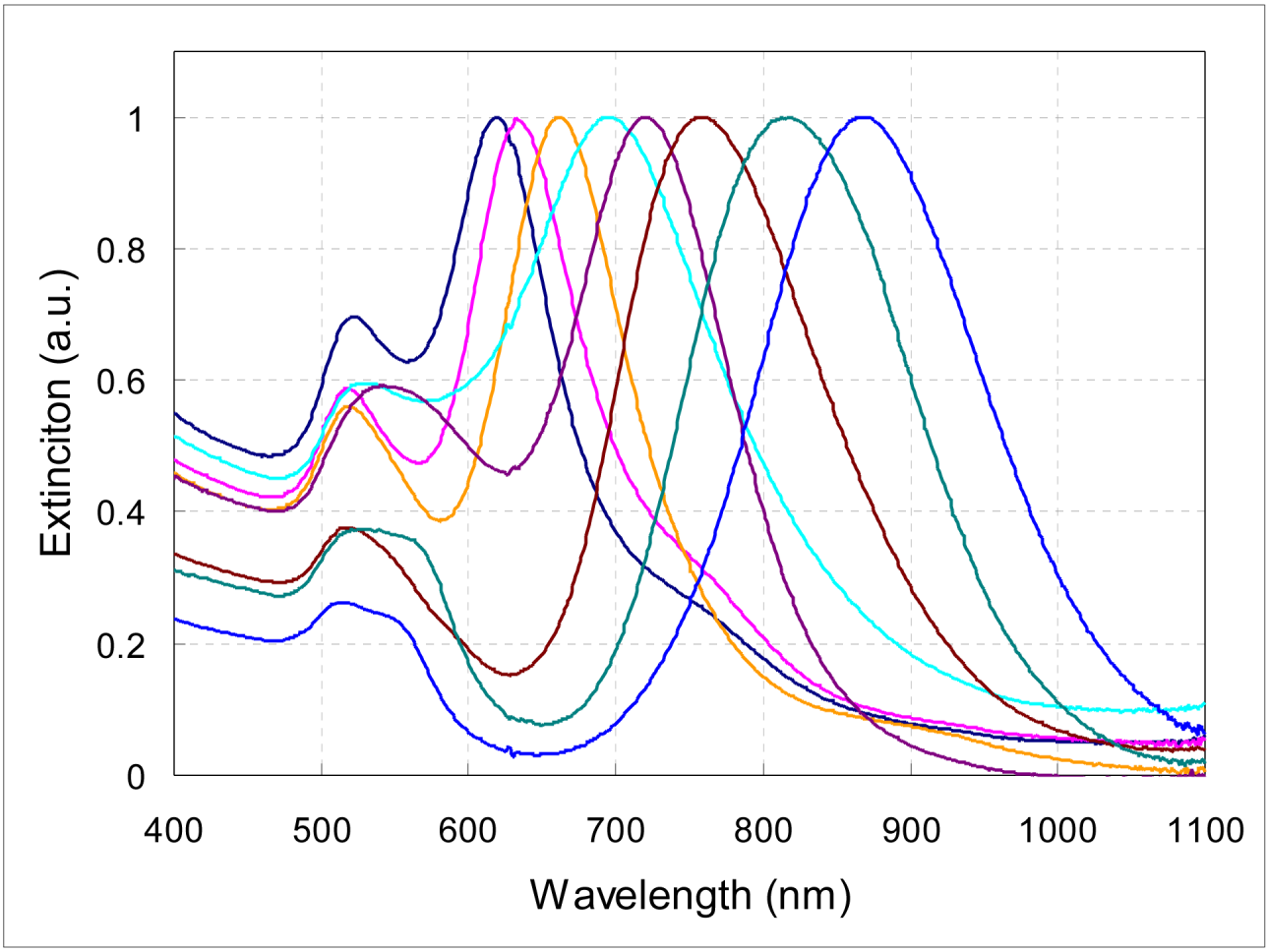

Figure 1.
Normalized absorption spectra of Au NRs with different longitudinal resonance peaks.

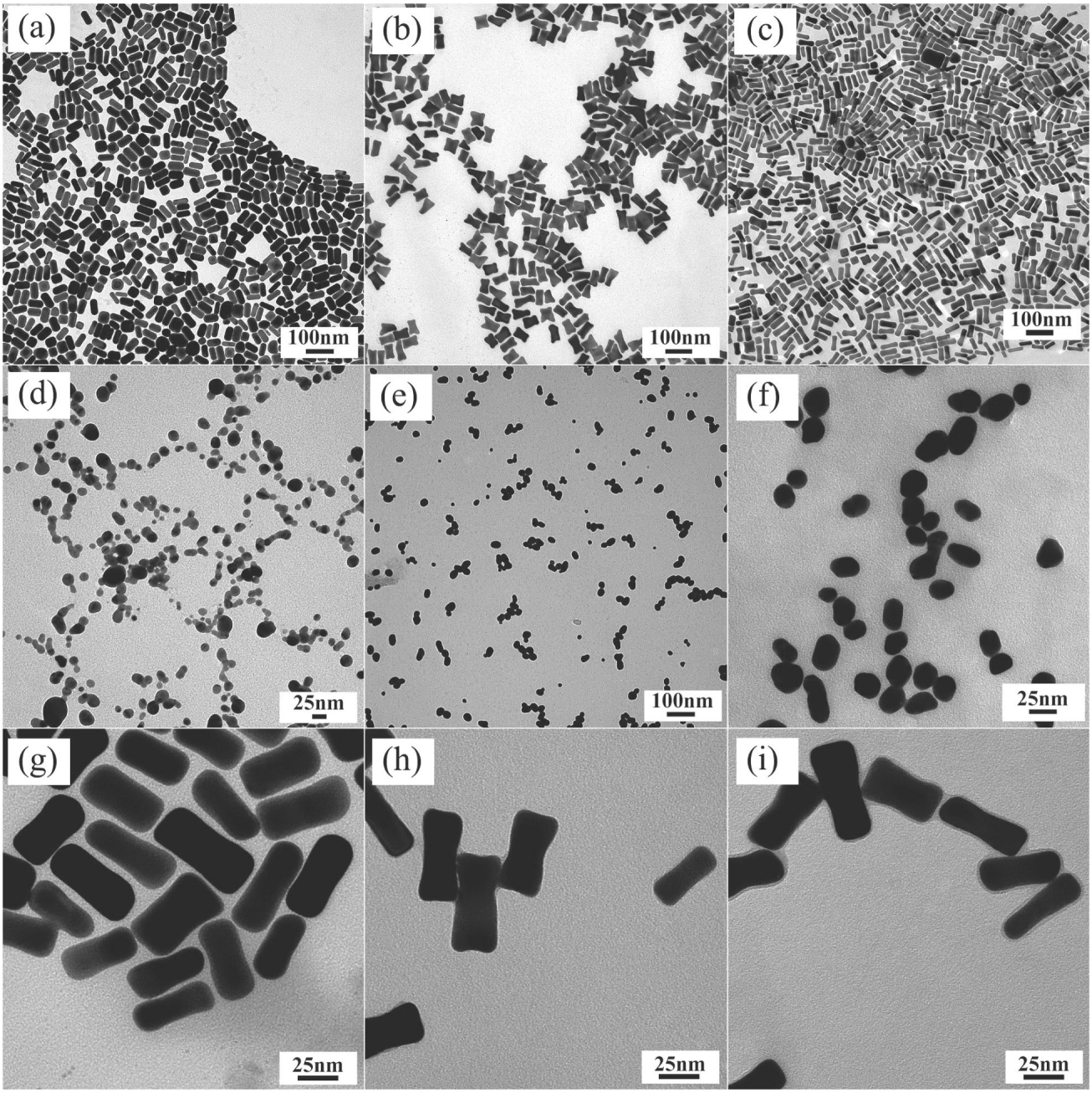

Figure 2.

TEM images of different nanoparticles. (a)~(c) gold nanorods (Au NRs) with different aspect ratios R=2.4, 1.9 and 3.0, respectively, (d) Silver nanoparticles (Ag NPs), (e) Au NPs, (f) Au NPs coated with positive charged polyelectrolyte (Au (+)pdNPs), (g) Au NRs capped by CTAB, (h) Au NPs coated with negative charged polyelectrolyte (Au (-)peNRs) and (i) Au NRs coated with positive charged polyelectrolyte (Au (+)pdNRs).

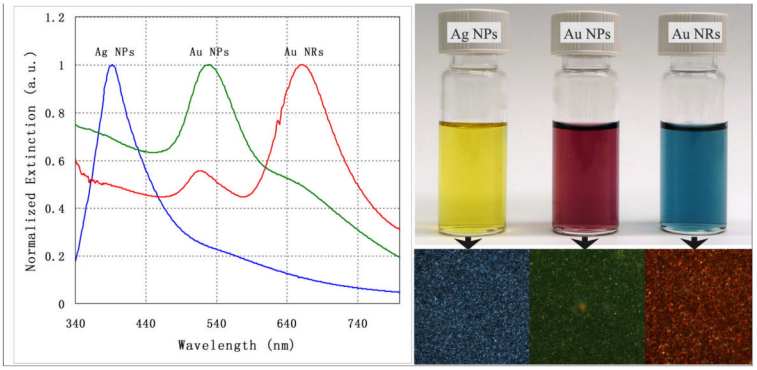

Figure 3.
Absorption spectra (left) and corresponding light scattering images (right) of the functionalized Au NRs, Au NPs and Ag NPs.

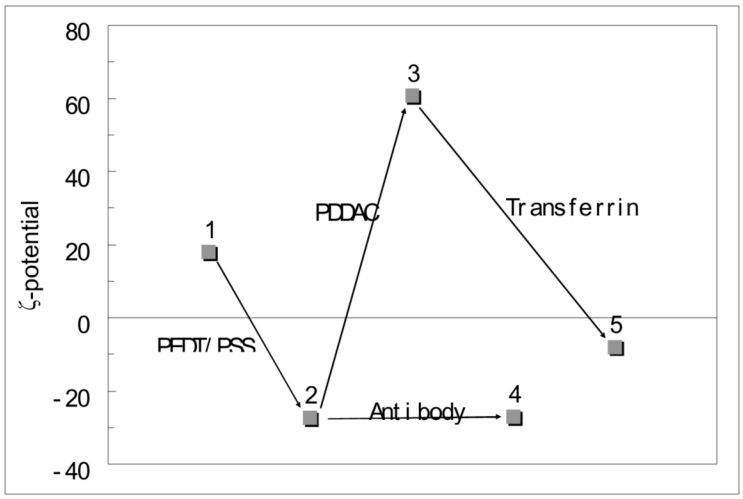

Figure 4.
ζ-potential of the Au NRs before and after functionalization and conjugation, where the numbers from 1~5 stands for CTAB stabilized Au NRs, Au (-)peNRs, Au (+)pdNRs, anti-mesothelin-conjugated Au (-)peNRs and Tf-conjugated Au (+)pdNRs, respectively.

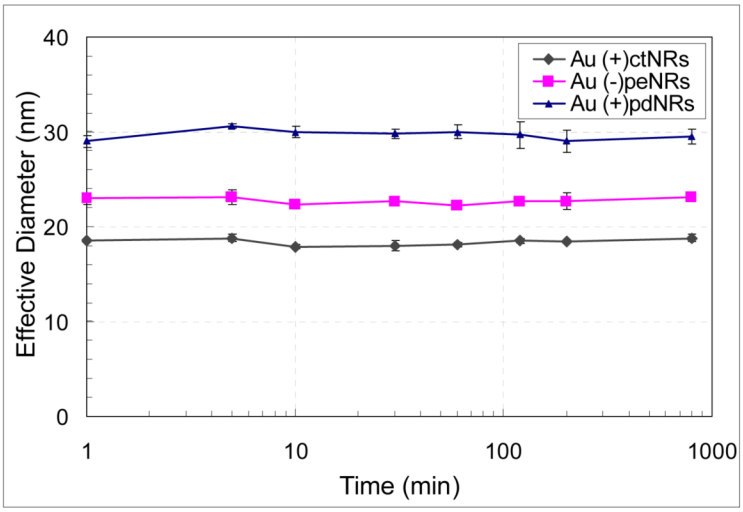

Figure 5.
Time-dependent profile of the effective diameter of the Au (+)ctNRs, (-)peNRs and (+)pdNRs.

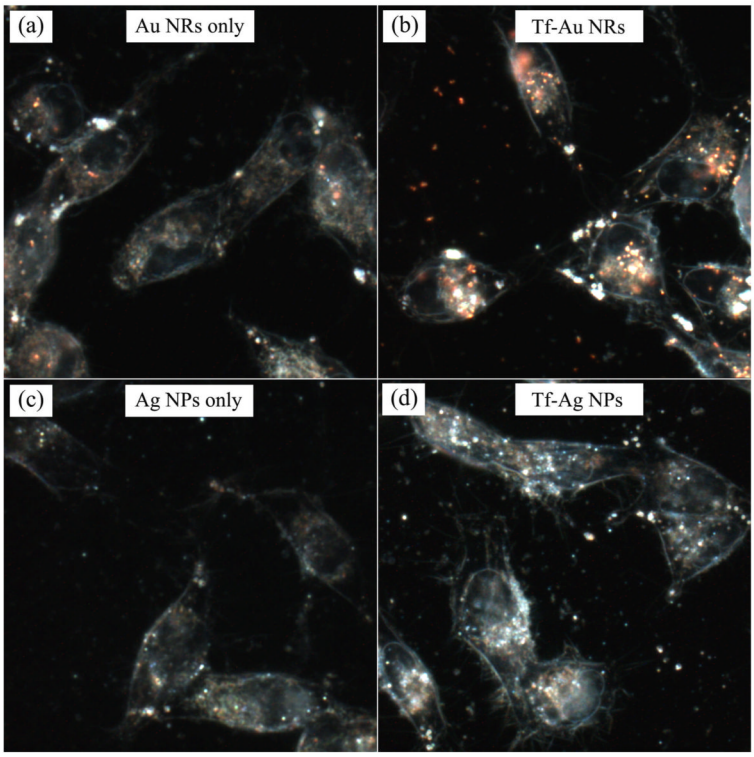

Figure 6.
MiaPaCa cells stained with Tf-Au (+)pdNRs or Tf-Ag (+)pdNPs bioconjugates.

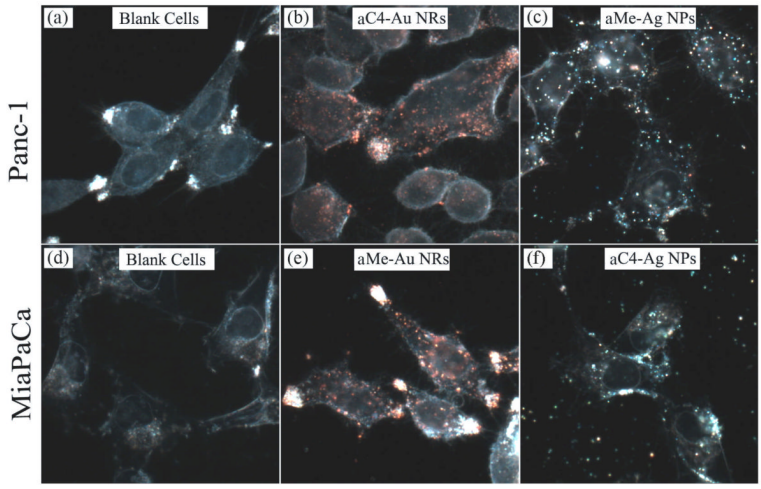

Figure 7.
Labeling of Panc-1 and MiaPaCa cells with antibody conjugated nanoparticles.

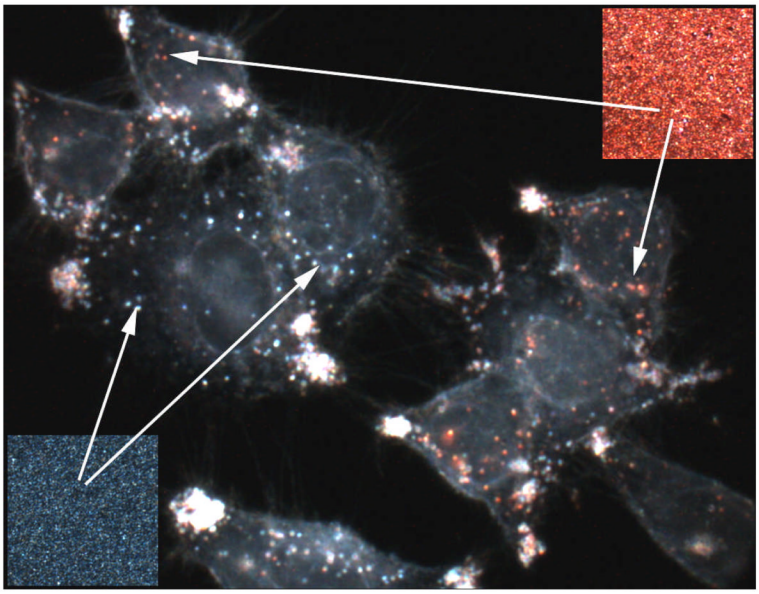

Figure 8.
Multiplexed imaging of Panc-1 cells labeled with antibody conjugated Au NRs and Ag NPs. Two insets are dark field images taken from Au NRs (up-right) and Ag NPs (bottom-left) on a glass slide.

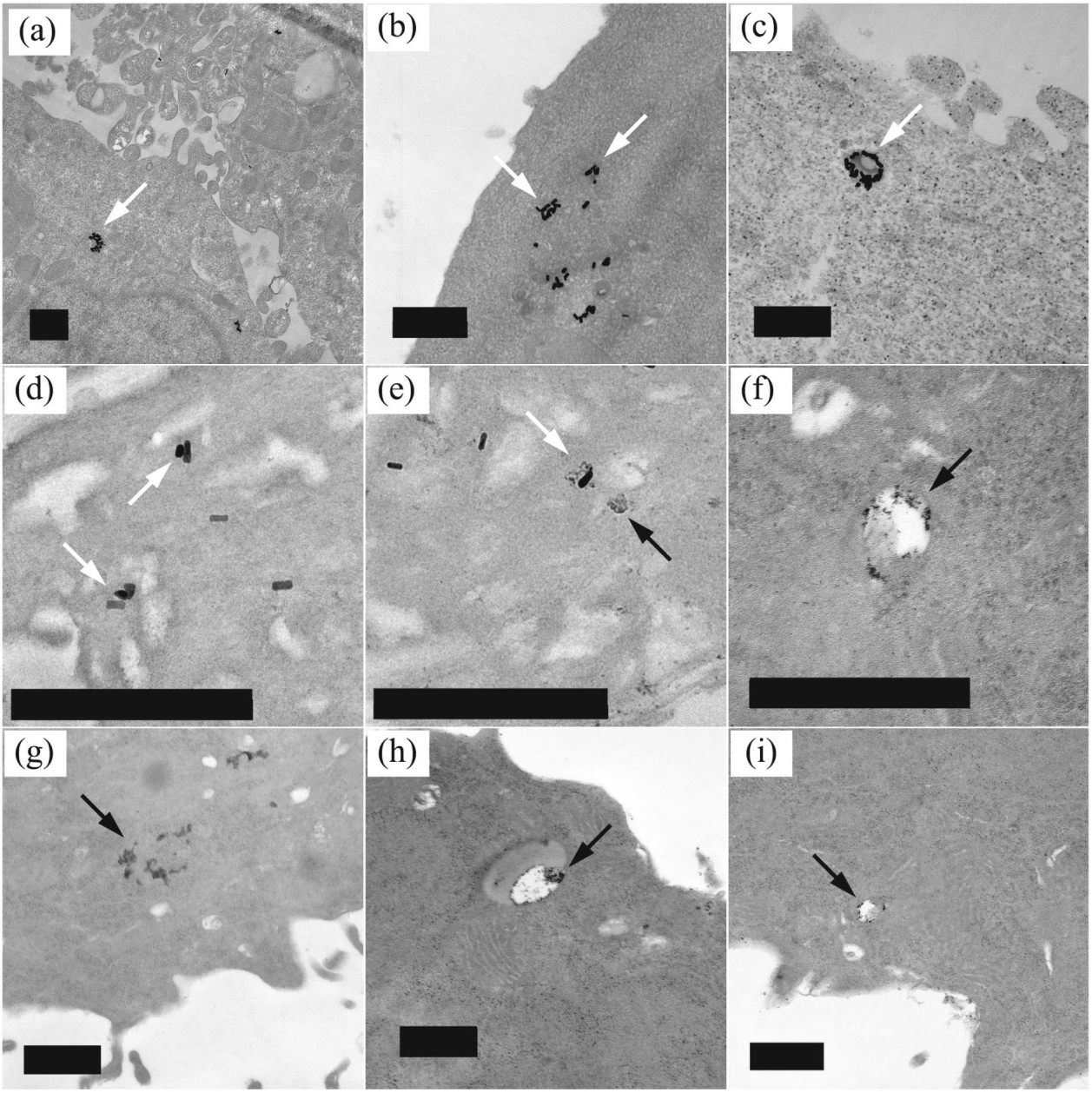

Figure 9.
TEM images of Panc-1 cells treated with aMe-Au NRs (white arrow) and aMe-Ag NPs (black arrow). The scale bars represent 500nm.

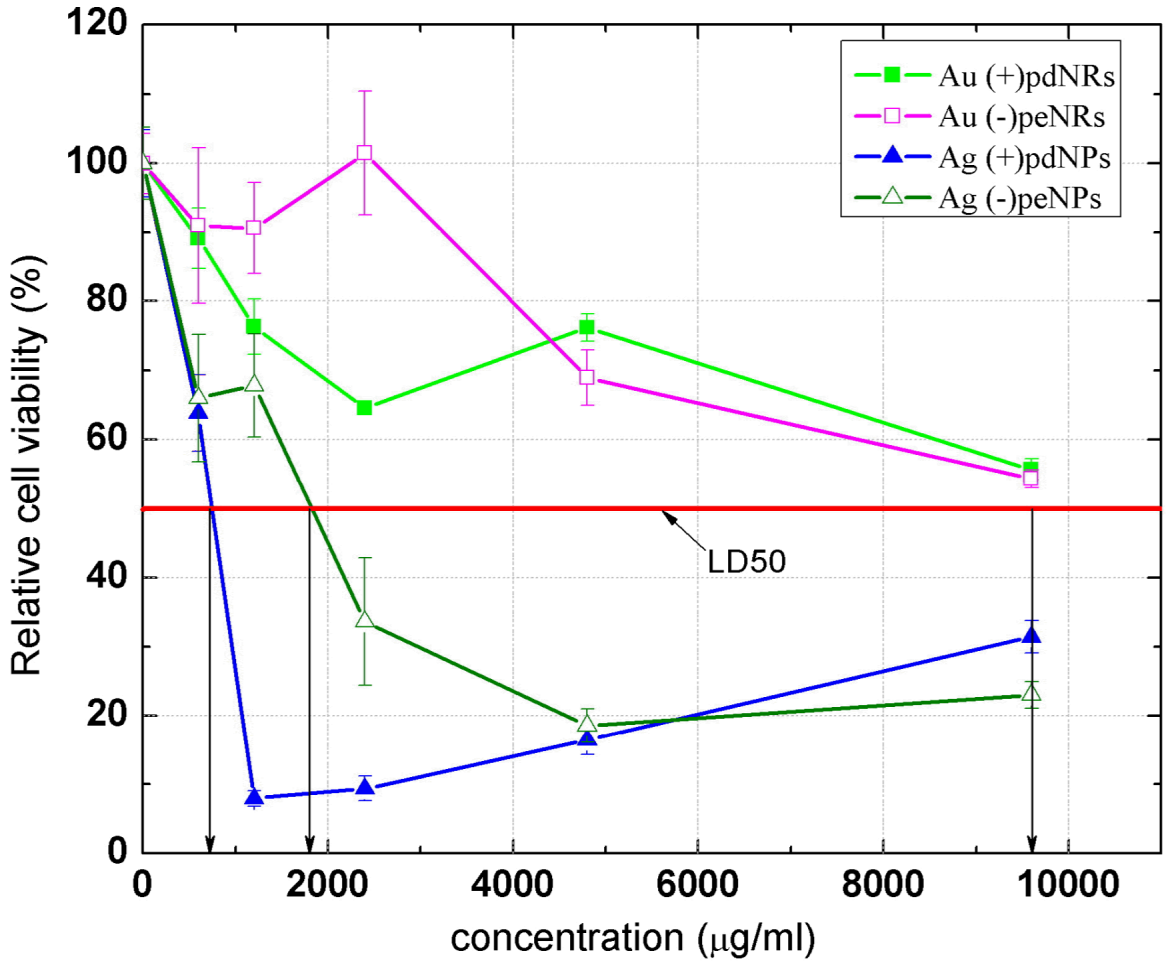

Figure 10.
Relative cell viability of cells treated with different kind of bioconjugates (48hrs). Statistical analysis shows that the values from Au NRs are mean ± S.D. (n = 4) $P < 0.05$ as compared to Ag NPs.